Chinese Chemical Letters 34 (2023) 107968

Contents lists available at ScienceDirect

Chinese Chemical Letters

journal homepage: www.elsevier.com/locate/cclet

Latest progress on fully non-fused electron acceptors for high-performance organic solar cells

Jianhong Gao[a,1], Xiaodong Zhu[a,1], Hanyi Bao[a], Jibao Feng[a], Xiang Gao[a,*], Zhitian Liu[a,*], Ziyi Ge[b,c,*]

[a] Hubei Engineering Technology Research Center of Optoelectronic and New Energy Materials, Hubei Key Laboratory of Plasma Chemistry and Advanced Materials, School of Materials Science and Engineering, Wuhan Institute of Technology, Wuhan 430205, China
[b] Ningbo Institute of Materials Technology and Engineering, Chinese Academy of Sciences, Ningbo 315201, China
[c] Center of Materials Science and Optoelectronics Engineering, University of Chinese Academy of Sciences, Beijing 100049, China

ARTICLE INFO

Article history:
Received 23 August 2022
Revised 10 October 2022
Accepted 31 October 2022
Available online 1 November 2022

Keywords:
Organic solar cells
Fully non-fused electron acceptors
Noncovalent interaction
Power conversion efficiency
Over 10%

ABSTRACT

Benefitting from the development of non-fullerene acceptors (NFAs), remarkable advances have been achieved with the power conversion efficiency (PCE) exceeding 19% over the last few years. However, the major achievement comes from fused ring electron acceptors (FREAs) with complex structures, leading to high cost. Hence, it is urgent to design new materials to resolve the cost issues concerning basic commercial requirements of organic solar cells. Recently, great progress has been made in fully non-fused ring electron acceptors (NFREAs) with only single-aromatic ring in the electron-donating core, which might achieve a fine balance between the efficiency and cost, thus accelerating the commercial application of organic solar cells. Therefore, this article summarizes the recent advances of fully NFREAs with efficiency over 10%, which may provide a guidance for developing the cost-effective solar cells.

1. Introduction

Organic solar cells (OSCs) have emerged as the most advanced one towards commercial applications with great potential for portable, wearable, and transparent devices [1–5]. Over the past few years, the power conversion efficiency (PCE) galloped ahead because of the development of fused ring electron acceptors (FREAs) [6–15]. In general, the FREAs are characterized by the acceptor-donor-acceptor (A-D-A) molecular backbone, in which D represents the electron-donating molecular core, and A represents the electron-withdrawing end group. Typically, a multi ring-fused ladder structure, ranging from five to eleven- (or more) membered rings, is used as the donor core, and 1,1-dicyanomethylene-3-indanone (IC) derivatives are served as the terminal electron deficient groups, such as the famous ITIC [16], IDIC [17], IEICO-4F [18], COi8DFIC [19], DTDP-IC [20], BT-IC [21], Y6 [22], N3 [23] and their analogues [24–26]. Currently, the PCE of single junction OSCs based on FREAs has exceeded 19% [27–31]. Despite exciting performance has been made, the access of such fused ladder structure usually involves multiple-step reactions and purification which inevitably increases synthetic complexities and costs. However, effective commercialization of OSCs need the photovoltaic materials to be as cheap as possible. Hence, it is urgent to explore the new electron acceptors (EAs) with low synthetic complexity.

Introducing noncovalent interaction (O···H, O···S, S···N, *etc.*) among aromatic units instead of chemical bonds is an effective strategy to lock the molecular configuration, which can mediate the planar geometry of π-conjugated skeleton and reduce the synthesis costs [32–34]. On the basis of this idea, non-fused ring electron acceptors (NFREAs) have been designed, so as to simplify the synthesis [35–40]. In general, NFREAs are developed with partially or fully non-fused structures depending on whether or not there is fused-ring in the donor core. From fused-ring to semi-fused ring and then to fully non-fused ring, reducing synthesis complexities were achieved by gradually tailoring the highly π-conjugated cores into tricycle or single aromatic units (Fig. 1a). Especially, fully NFREAs could be constructed based on the single aromatic ring, such as benzene and thiophene, in the central donor moiety. Recently, the combinational efforts from structure modification and device optimization have rapidly boosted the PCE over 15% [41]. This is a great achievement in the development of high-efficiency and low cost fully NFREAs, and will bring the fully NFREAs under the

* Corresponding authors.
E-mail addresses: xgao@wit.edu.cn (X. Gao), able.ztliu@wit.edu.cn (Z. Liu), geziyi@nimte.ac.cn (Z. Ge).
[1] These authors contributed equally to this work.

https://doi.org/10.1016/j.cclet.2022.107968
1001-8417/

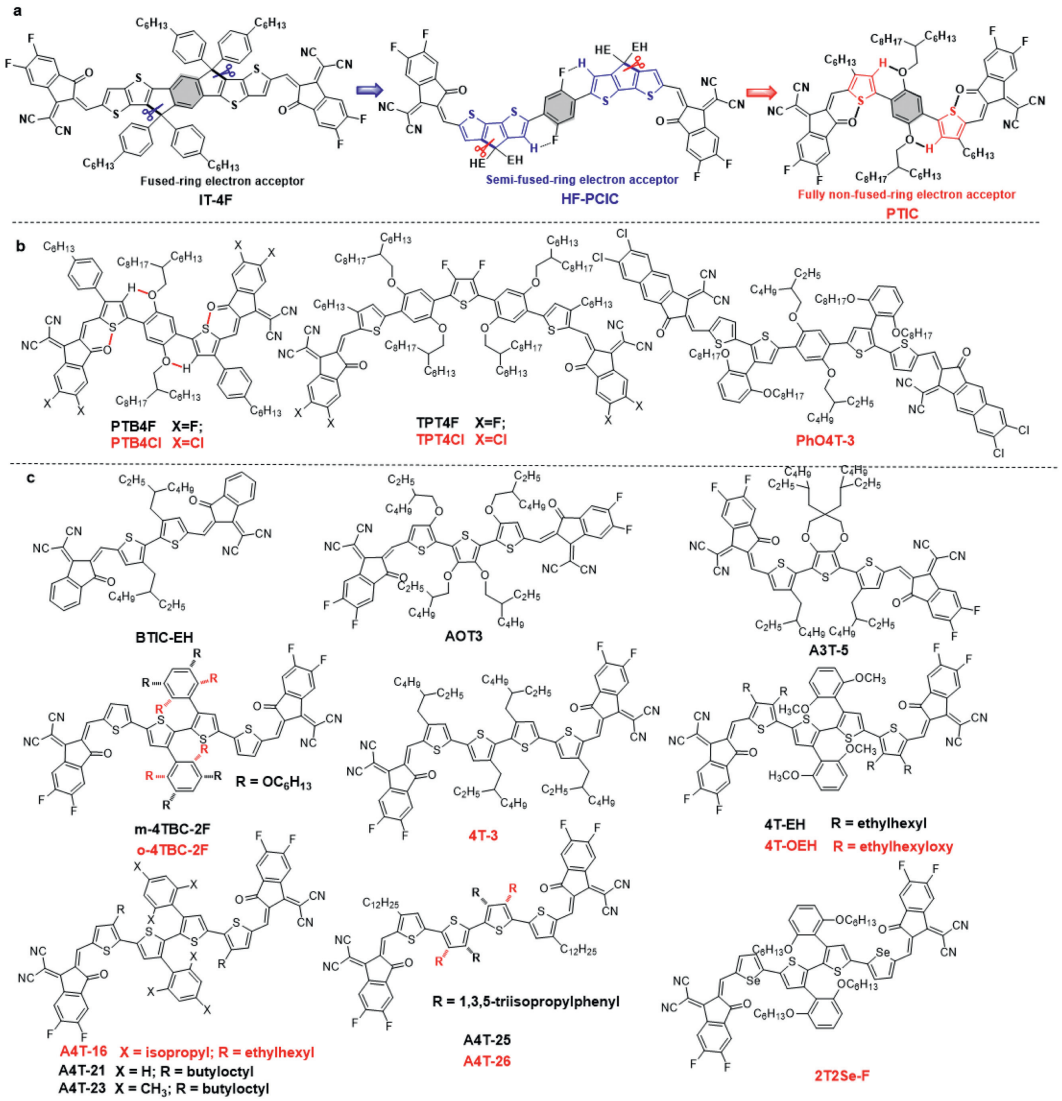

Fig. 1. (a) Molecular Structures of FREA IT-4F, semi-FREA HF-PCIC and fully NFREA PTIC. (b) Molecular Structures of fully NFREAs with benzene and thiophene rings. (c) Molecular Structures of fully NFREs with oligothiophene. EH 2-ethylhexyl.

spotlight. This review briefly summarizes high-efficiency fully NFREAs with PCE over 10%.

2. Molecular skeleton

In terms of chemical structure, FREAs can be classified into three parts: molecular skeleton, terminal, and side chain. Among them, side chain and terminal can endow the molecular with good solubility and induce intramolecular charge transfer, respectively. Meanwhile, the molecular skeleton can easily form planar conformation thanks to fused-ring core, which facilitates charge transport, and thus yielding excellent photovoltaic performance. However, the multi-ring fused core structure inevitably involves complex synthesis steps, resulting in low overall yields and high synthetic costs. Fortunately, recent research has demonstrated that construction of the non-fused backbone by utilizing non-covalent interaction could also maintain the highly co-planar conformation among aromatic units while reducing the material costs. Especially for completely structural simplification, fully NFREAs were developed with simpler aromatic rings, including benzene and thiophene rings or multi-thiophene rings, as the molecular skeleton. Such a simple molecular structure can be obtained *via* three steps, which connecting the core with the π-bridge units through C-H activation reaction, and then introducing the aldehyde group on both side of π-bridge units through Vilsmeier-Hacck reaction, and finally connecting the terminal through Knoevenagel condensation reaction. Compared with FREAs (*e.g.*, Y6 approximately contains 10 steps), simplified synthesis complexities (only 3 steps) of fully NFREAs provide the possibility for practical application. According to the types of building blocks in the core moiety, fully NFREAs are divided into two categories: (1) benzene and thiophene rings, and (2) oligothiophene.

2.1. Benzene and thiophene rings

In 2019, Chen and coworkers reported the first high performance fully NFREA with the thiophene and phenyl backbone, realizing the PCE over 10% by taking advantage of noncovalently conformational locking strategy [42]. This high performance and simple fully non-fused 2,2′-((2*Z*,2′*Z*)-(((2,5-bis((2-hexyldecyl)oxy)-1,4-phenylene)bis(3-hexylthiophene-5,2-diyl))bis(methanylylidene))bis(5,6-difluoro-3-oxo-2,3-dihydro-1*H*-indene-2,1-diylidene))dimalononitrile (PTIC) (Fig. 1a) are obtained by a two-step synthetic routes, and purified by recrystallization without column

purification. Compared with the FREA 2,2′-((2*Z*,2′*Z*)-((4,4,9,9-tetrakis(2-ethylhexyl)-4,9-dihydro-s-indaceno[1,2-b:5,6-b′]dithiophene-2,7-diyl)bis(methanylylidene))bis(5,6-difluoro-3-oxo-2,3-dihydro-1*H*-indene-2,1-diylidene))dimalononitrile (ID4F), the synthetic complex index of PTIC is only 56.7% of that of ID4F. The geometry of PTIC is locked into a planar conformation with dense "end-to-end" stacking in solid owing to intramolecular noncovalent interaction. Therefore, the high crystallinity and ordered stacking could be formed in both neat and blend films, which were also be confirmed by grazing incidence wide-angle X-ray scattering (GIWAXS) experiments. As a result, decent PCEs of 10.27% and 13.97% were achieved in single-junction and tandem OSCs, respectively. Moreover, the corresponding device maintained about 70% of original PCE under continuous illumination for 50 h, which may stem from the structure factors of PTIC without extension-fused ring and tetrahedron sp^3 bridge carbon. To further explore the relationship between photostability and structure factors, the representative molecular skeletons of A-D-A non-fullerene acceptors (NFAs) with the fused (5,5,11,11-tetrakis(4-hexylphenyl)-dithieno[2,3-*d*:2′,3′-*d*′]-s-indaceno[1,2-*b*:5,6-*b*′]dithiophene)bis(5,6-difluoro-3-oxo-2,3-dihydro-1*H*-indene-2,1-diylidene)dimalononitrile(IT-4F), semi-fused 2,2′-((2*Z*,2′*Z*)-(((2,5-difluoro-1,4-phenylene)bis(4,4-bis(2-ethylhexyl)-4*H*-cyclopenta[2,1-*b*:3,4-*b*′]dithiophene-6,2-diyl))bis(methanylylidene))bis(5,6-difluoro-3-oxo-2,3-dihydro-1*H*-indene-2,1-diylidene))dimalononitrile (HF-PCIC), and non-fused cores (PTIC) were selected as studying examples to investigate the photodegradation pathway (Fig. 1a) [43]. The single-crystal structure revealed that PTIC adapts the "brick-like" end to end packing with short π-π distance, which was consistent with the GIWAXS measurements where PTIC possesses the tightest π-π stacking distance among these samples (Fig. 2a). The close stacking of PTIC could be attributed to its sp^3 carbon-free planar backbone compared with IT-4F and HF-PCIC. Meanwhile, it clearly observed that the introduction of outward hexyl chain in the thiophene bridge effectively suppresses the photoisomerization of the vinyl group by performing single-crystal analysis of two model molecules, (*Z*)-2-(5,6-difluoro-2-((3-hexylthiophen-2-yl)methylene)-3-oxo-2,3-dihydro-1*H*-inden-1-ylidene)malononitrile (TFIC) and (*Z*)-2-(5,6-difluoro-3-oxo-2-(thiophen-2-ylmethylene)-2,3-dihydro-1*H*-inden-1-ylidene)malononitrile (TFICH) from PTIC (Fig. 2b). These combined structure factors, including planar sp^3 carbon-free skeleton and hinder outward-chain, endow fully non-fused acceptors with the elongated excited lifetime and excellent photostability. Therefore, among the studied samples, fully non-fused PTIC displays superior photostability in solution, films, and solar cells. Obviously, non-fused PTIC-based OSCs showed about 359 times and 322 times slower decay rates than fused IT-4F and semi-fused HF-PCIC. Besides, the same group further improves the PCE of single-junction OSCs to 12.76% based on 2,2′-((2*Z*,2′*Z*)-(((2,5-bis((2-hexyldecyl)oxy)-1,4-phenylene)bis(3-(4-hexylphenyl)thiophene-5,2-diyl))bis(methanylylidene))bis(5,6-dichloro-3-oxo-2,3-dihy-dro-1*H*-indene-2,1-diylidene))dimalononitrile (PTB4Cl) (Fig. 1b), which was synthesized *via* modifying the terminal side chain and screening the halogen atoms in IC derivatives [44]. This result proves that introduction of two-dimensional chains and halogenated terminals could effectively regulate the solid-state properties of full NFREAs, thus extending the exciton lifetime and promoting the fast charge transfer. With the above information in hands, this group have further designed two medium bandgap electron acceptors by using muti-noncovalent interaction (O···S, O···H and F···H) between molecular skeleton and end groups [45]. These non-fused acceptors exhibit the relatively planar and rigid conformation, and the 2,2′-((2*Z*,2′*Z*)-((((3,4-difluorothiophene-2,5-diyl)bis(2,5-bis((2-hexyldecyl)oxy)-4,1-phenylene))bis(3-hexylthiophene-5,2-diyl))bis(methanylylidene))bis(5,6-dichloro-3-oxo-2,3-dihydro-1*H*-indene-2,1-diylidene))dimalononitrile (TPT4Cl) (Fig. 1b) achieved a higher PCE of 10.16% relative to the 2,2′-((2*Z*,2′*Z*)-((((3,4-difluorothiophene-2,5-diyl)bis(2,5-bis((2-hexyldecyl)oxy)-4,1-phenylene))bis(3-hexylthiophene-5,2-diyl))bis(methanylylidene))bis(5,6-difluoro-3-oxo-2,3-dihydro-1*H*-indene-2,1-diylidene))dimalononitrile (TPT4F, 7.67%) with a low non-radiative loss of 0.27 eV, due to the more ordered face-on stacking and stronger photoluminescence in solid films.

Recently, Li *et al*. reported the synthesis of three fully NFREAs type electron acceptors by adopting commercially available 2,3-dibromothiophene as the starting material [46]. Expanding the π-conjugated skeleton and modifying the end-groups systematically regulate light-harvesting ability, energy levels, and packing behaviors in the solid state. As a result, the 2,2′-((2*Z*,2′*Z*)-(((2,5-bis((2-ethylhexyl)oxy)-1,4-phenylene)bis(3′-(2,6-bis(octyloxy)phenyl)-[2,2′-bithiophene]-5′,5-diyl))bis(methanylylidene))bis(6,7-dichloro-3-oxo-2,3-dihydro-1*H*-cyclopenta[*b*]naphthalene-2,1-diylidene))dimalononitrile (PhO4T-3) (Fig. 1b) exhibits the champion PCE of 13.76%, which is the record PCE of fully NFREAs including the phenyl in molecular skeleton so far.

2.2. Oligothiophene

In addition, a series of fully NFREAs based on oligothiophene core with different numbers of thiophene units have been designed and synthesized to modify their photovoltaic performance. For instance, Li *et al*. reported the fully non-fused acceptor, 2,2′-((2*Z*,2′*Z*)-((3,3′-bis(2-ethylhexyl)-[2,2′-bithiophene]-5,5′-diyl)bis(methanylylidene))bis(3-oxo-2,3-dihydro-1*H*-indene-2,1-diylidene)) dimalononitrile (BTIC-EH), with the least thiophene rings (2,2′-bithiophene), as the central skeleton shows a PCE of 2.4% [47]. A relatively low PCE is mainly attributable to limited conjugated length. Therefore, trithiophene was used as the central electron-donating unit to construct simple acceptors for enlarge the conjugated length, *e.g*., 2,2′-((2*Z*,2′*Z*)-((3,3′,3″,4′-tetrakis((2-ethylhexyl)oxy)-[2,2′:5′,2″-terthiophene]-5,5″-diyl)bis(methanylylidene))bis(5,6-difluoro-3-oxo-2,3-dihydro-1*H*-indene-2,1-diylidene))dimalononitrile (AOT3) reported by Yao *et al*. [48] and 2,2′-((2*Z*,2′*Z*)-(((3,3-bis(2-ethylhexyl)-3,4-dihydro-2*H*-thieno[3,4-*b*][1,4]dioxepine-6,8-diyl)bis(4-(2-ethylhexyl)thiophene-5,2-diyl))bis(methanylylidene))bis(5,6-difluoro-3-oxo-2,3-dihydro-1*H*-indene-2,1-diylidene))dimalononitrile (A3T-5) reported by Zhu *et al*. [49]. Obviously, an increase of J_{sc} could be obtained, and high PCEs of 6.59% and 7.03% were achieved in the AOT3- and A3T-5-based OSCs, respectively. Encouraging, further increasing the thiophene unit of donor core, tetrathiophene, superior performances have been obtained compared with bithiophene and trithiophene. In 2020, Chen *et al*. designed and synthesized two fully NFREAs of 2,2′-((2*Z*,2′*Z*)-((3″,4′-bis(2,6-bis(hexyloxy)phenyl)-[2,2′:5′,2″:5″,2‴-quaterthiophene]-5,>5‴-diyl)bis(methanylylidene))bis(5,6-difluoro-3-oxo-2,3-dihydro-1*H*-indene-2,1-diylidene))dimalononitrile (*o*-4TBC-2F) and 2,2′-((2*Z*,2′*Z*)-((3″,4′-bis(3,5-bis(hexyloxy)phenyl)-[2,2′:5′,2″:5″,2‴-quaterthiophene]-5,5‴-diyl)bis(methanylylidene))bis(5,6-difluoro-3-oxo-2,3-dihydro-1*H*-indene-2,1-diylidene))dimalononitrile (*m*-4TBC-2F) (Fig. 1c) by changing the position of hexyloxy groups on the side phenyl [50]. The result of density functional theory (DFT) calculation displayed significantly different molecular geometries: the molecular backbone of *o*-4TBC-2F was quasi planar, while *m*-4TBC-2F was twisted. Therefore, the molecular orientation and stacking of *o*-4TBC-2F in pure and blend films were more ordered compared with *m*-4TBC-2F. Meanwhile, the energy loss and energetic disorder of *o*-4TBC-2F-based device are also lower. Finally, these excellent properties endowed the *o*-4TBC-2F with a high PCE of 10.26% after thermal annealing. They further optimized the side chain in the tetra-thiophene core [51]. It was found that the 2,2′-((2*Z*,2′*Z*)-((3″,4,4′,4‴-tetrakis(2-ethylhexyl)-[2,2′:5′,2″:5″,2‴-

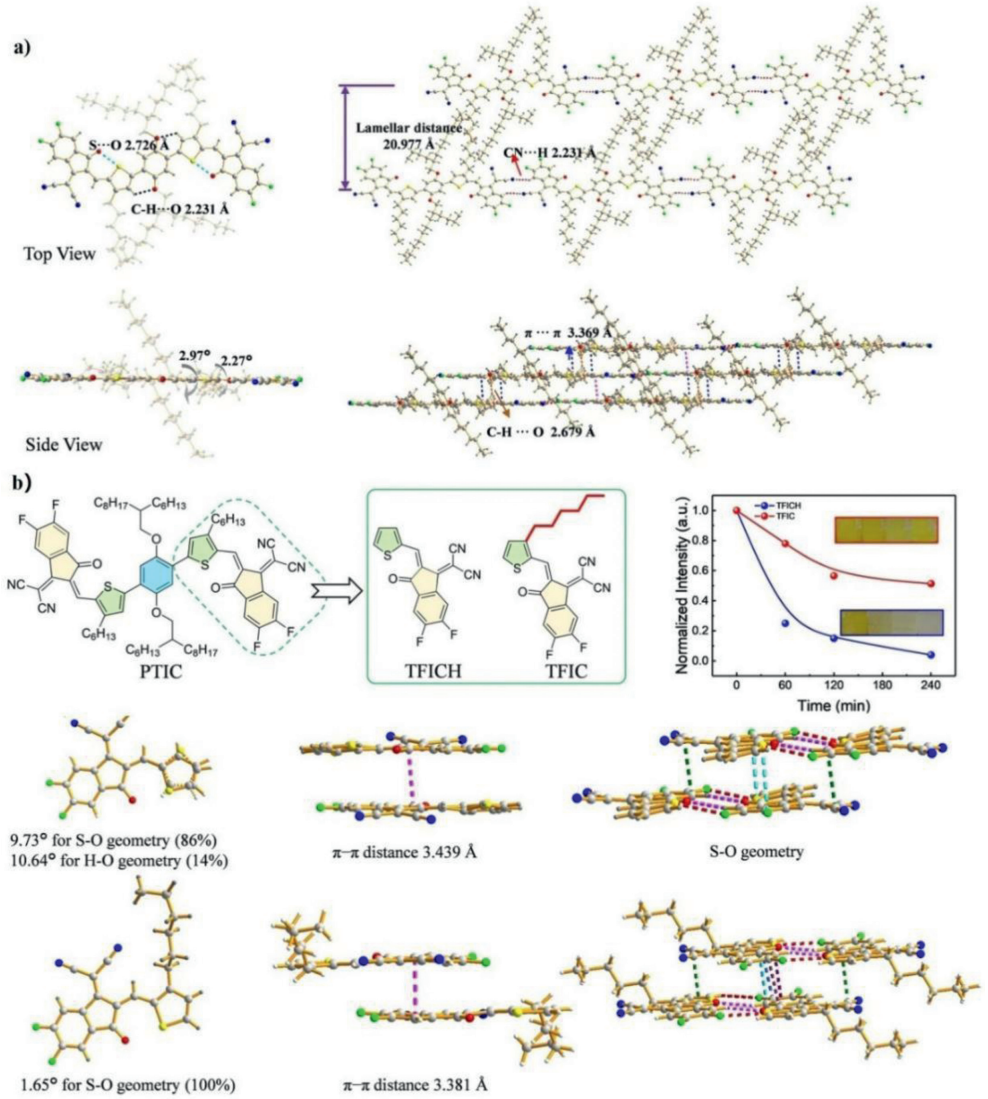

Fig. 2. (a) Molecular packing of PTIC in the single crystal structure. (b) Molecule structure and single-crystal structure of terminal models, TFICH, and TFIC from PTIC. Reproduced with permission [43]. Copyright 2021, Springer Nature.

quaterthiophene]-5,5‴-diyl)bis(methanylylidene))bis(5,6-difluoro-3-oxo-2,3-dihydro-1*H*-indene-2,1-diylid-ene))dimalononitrile (4T-3) (Fig. 1c) with four 2-ethylhexyl side chains could achieve an encouraging PCE of 10.15%, when the poly([4,8-bis(5-(2-ethylhexyl)thiophen-2-yl)benzo[1,2-*b*:4,5-*b*′]dithiophene-2,6-diyl]-alt-[1,3-bis(2-ethylhexyl)-5,7-di(thiophen-2-yl)-4*H*,8*H*-benzo[1,2-*c*:4,5-*c*′]dithiophene-4,8-dione-5,5-diyl]) (PBDB-T) was selected as the polymer donor. Interestingly, the PCE could even be improved as high as 12.04% based on D18:4T-3 device. This result demonstrates that the improved device performance could be achieved by regulating side chains to change the compatibility with these donor polymers. On this basis, the acceptor molecule of 2,2′-((2*Z*,2′*Z*)-((3″,4′-bis(2,6-dimethoxyphenyl)-3,3‴,4,4‴-tetrakis ((2-ethylhexyl)oxy)-[2,2′:5′,2″:5″,2‴-quaterthiophene]-5,5‴-diyl) bis(methanylylidene))bis(5,6-difluoro-3-oxo-2,3-dihydro-1*H*-indene -2,1-diylidene))dimalononitrile (4T-OEH) with 3,4-bis((2-ethyl hexyl)oxy) thiophene was designed by regulating the type of side chains [52]. Especially, given the existence of intramolecular S-O noncovalent interaction, the 4T-OEH (Fig. 1c) displays a planar molecular backbone. Thus, an excellent PCE of 12.12% could be achieved by blending with the PBDB-T.

Recently, Hou's group elevated the PCE of fully NFREAs up to 15.2% using tetrathiophene as the central donor core with bulky side chains [41]. They synthesized three fully NFREAs, 2,2′-((2*Z*,2′*Z*)-((3,3‴-bis(2-ethylhexyl)-3″,4′-bis(2,4,6-triisopropylphenyl)-[2,2′:5′,2″:5″,2‴-quaterthiophene]-5,5‴-diyl)bis (methanylylidene))bis(5,6-difluoro-3-oxo-2,3-dihydro-1*H*-indene-2,1-diylidene)) dimalononitrile (A4T-16), 2,2′-((2*Z*,2′*Z*)-((3,3‴-bis(2-butyloctyl)-3″,4′-diphenyl-[2,2′:5′,2″:5″,2‴-quaterthiophene]-5,5‴-diyl)bis(methanylylidene))bis(5,6-difluoro-3-oxo-2,3-dihydro-1*H*-indene-2,1-diylidene))dimalononitrile (A4T-21) and 2,2′-((2*Z*,2′*Z*)-((3,3‴-bis(2-butyloctyl)-3″,4′-dimesityl-[2,2′:5′,2″:5″,2‴-quater thiophene]-5,5‴-diyl)bis(methanylylidene))bis(5,6-difluoro-3-oxo-2,3-dihydro-1*H*-indene-2,1-diylidene))dimalononitrile (A4T-23) (Fig. 1c), by modifying the alkyl groups in the side phenyl groups, as shown in Table 1. The DFT calculation result shows that introduction of the group of 2,4,6-trimethylphenyl is not only more effective in enhancing the conformational stability, but also provide the steric hindrance for inducing the formation of the favorable intermolecular packing. Further, the single-crystal structure reveals that the molecular, AT-16, exhibited a three-dimensional interpenetrating network due to the compact π-π stacking between the adjacent end-capping groups, which is in

Table 1
Performance data of fully non-fused electron acceptors.

Acceptor	E_g^{opt} (eV)	Donor	J_{SC} (mA/cm^2)	V_{OC} (V)	FF	PCE (%)	V_{loss} (V)	Ref.
PTIC	1.53	PBDB-TF	16.73	0.93	0.66	10.27	0.58	[42]
PTB4Cl	1.58	PBDB-TF	19.01	0.93	0.72	12.76	0.61	[44]
PTB4F	1.65	PBDB-TF	14.55	0.94	0.51	7.04	0.67	[44]
TPT-4Cl	1.67	PBDB-TF	15.77	1.04	0.62	10.16	0.61	[45]
TPT-4F	1.69	PBDB-TF	13.36	1.00	0.57	7.67	0.68	[45]
PhO4T-3	1.49	PBDB-T	23.03	0.84	0.71	13.76	0.62	[46]
BTIC-EH	1.64	PBDB-T	6.33	0.71	0.54	2.40	-	[47]
AOT3	1.22	PCE10	17.63	0.62	0.59	6.59	-	[48]
A3T-5	1.43	PBDB-TF	15.3	0.85	0.54	7.03	-	[49]
o-4TBC-2F	1.47	PBDB-T	20.48	0.76	0.66	10.26	0.63	[50]
m-4TBC-2F	1.66	PBDB-T	7.96	0.84	0.40	2.63	0.84	[50]
4T-3	1.52	PBDB-T	17.27	0.81	0.72	10.15	0.67	[51]
4T-3	1.52	D18	18.28	0.93	0.71	12.04	0.59	[51]
4T-OEH	1.44	PBDB-T	21.78	0.85	0.65	12.12	0.53	[52]
4T-EH	1.48	PBDB-T	15.02	0.91	0.54	7.36	0.59	[52]
AT-16	1.51	PBDB-TF	21.80	0.88	0.80	15.2	0.63	[41]
AT-21	1.74	PBDB-TF	5.55	0.94	0.30	1.57	0.80	[41]
AT-23	1.49	PBDB-TF	21.00	0.87	0.57	10.4	0.62	[41]
AT-25	1.39	PBDB-TF	17.2	0.90	0.51	7.83	0.59	[53]
AT-26	1.46	PBDB-TF	18.9	0.86	0.72	12.10	0.69	[53]
2T2Se-F	1.44	PBDB-TF	20.63	0.88	0.67	12.17	-	[58]

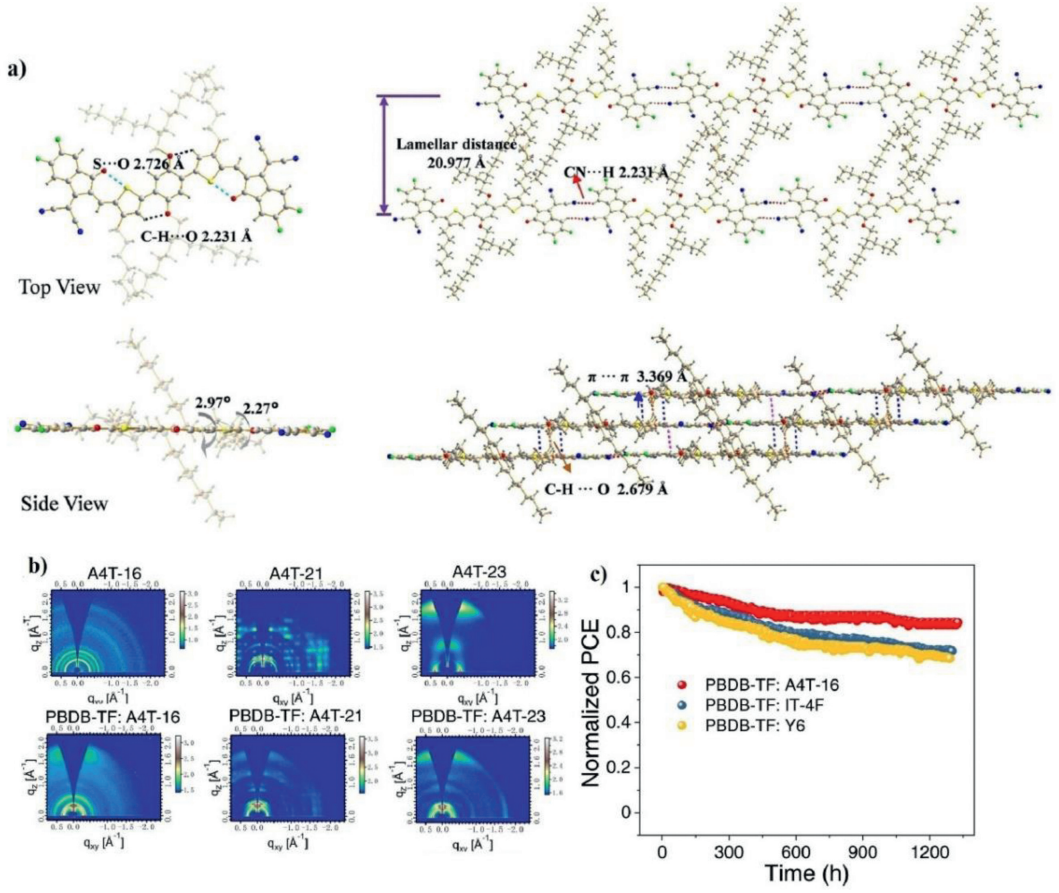

Fig. 3. (a) Molecular packing of A4T-16 in the single crystal structure. (b) GIWAXS patterns of the A4T-16, A4T-21, A4T-23 pure and blend films, respectively. (c) Photostability of IT-4F-, Y6- and A4T-16-based cells. Reproduced with permission [41]. Copyright 2021, Springer Nature.

agreement with the GIWAXS measurement results (Figs. 3a and b). Moreover, the 3D network of AT-16-based blend film could still be observed compared with others (Fig. 3b). The electroluminescent external quantum efficiency of A4T-16 and the Urbach energy of OSCs based on blend of A4T-16 and poly([4,8-bis(5-(2-ethylhexyl)-4-fluorothiophen-2-yl)benzo[1,2-*b*:4,5-*b*′]dithiophene-2,6-diyl]-alt-[1,3-bis(2-ethylhexyl)-5,7-di(thiophen-2-yl)-4*H*,8*H*-benzo[1,2-*c*:4,5-*c*′]dithiophene-4,8-dione-5,5-diyl]) (PBDB-TF) are comparable with Y6. Therefore, a best PCE of 15.2% could be achieved based on PBDB-TF:AT-16 with a very low non-radiative energy loss of only 0.214 eV. What is more, the device shows good stability: retaining 84% of its initial PCE after 1300 h under the simulated AM 1.5 G illumination (Fig. 3c). In addition, the decent PCEs over 10% could also be acquired with a few representative polymer donors, indicating its good universality. Subsequently, intermolecular aggregation properties were

further studied by introducing the triisopropylphenyl into different position of the central thiophene units [53]. The single crystal structure analysis and the transfer integral calculation show more compact π-π stacking in 2,2′-((2*Z*,2′*Z*)-((4,4‴-didodecyl-3′,4″-bis(2,4,6-triisopropylphenyl)-[2,2′:5′,2″:5″,2‴-quaterthiophene]-5,5‴-diyl)bis(methanylylidene))bis(5,6-difluoro-3-oxo-2,3-dihydro-1*H*-indene-2,1-diylidene))dimalononitrile (*A*4T-26), which promote efficient charge transportation compared to that in 2,2′-((2*Z*,2′Z)-((4,4‴-didodecyl-3″,4′-bis(2,4,6-triisopropylphenyl)-[2,2′:5′,2″:5″,2‴-quaterthiophene]-5,5‴-diyl) bis(methanylylidene))bis(5,6-difluoro-3-oxo-2,3-dihydro-1*H*-indene -2,1-diylidene))dimalononitrile (A4T-25) (Fig. 1c). Therefore, the photovoltaic performance based on PBDB-TF:A4T-26 yields an enhanced PCE of 12.1%. Beside constructing the noncovalent interaction of S-O, introduction of Se atom is also an effective way to enhance molecular packing *via* forming Se-Se noncovalent interaction [54–57]. Ding *et al.* developed a fully unfused acceptor, 2,2′-((2*Z*,2′*Z*)-(((3,3′-bis(2,6-bis(hexyloxy)phenyl)-[2,2′-bithiophene]-5,5′-diyl)bis(selenophene-5,2-diyl))bis(methanylylidene))bis(5,6 -difluoro-3-oxo-2,3-dihydro-1*H*-indene-2,1-diylidene))dimalono nitrile (2T2Se-F) (Fig. 1c), using selenophene to link bithiophene core with terminal groups [58]. The crystal structure clearly demonstrates a unique interpenetrating network with multiple intermolecular π-π interactions, thus obtaining a high PCE of 12.17%. It turns out that multiple conformation locking and large steric hindrance are effective in planarizing the backbone, which is beneficial to improve the PCE.

3. Summary

In summary, the PCE based on fully NFREAs has exceeding 15%, whereas it still falls behind FREAs (over 19%). However, considering the low synthetic complexity and great promise for future industrial application, more efforts should be made to study the structure-performance relationship and the compatibility with donor polymers. On the basis of current research, the follow principles should be comprehensively considered for improving efficiency of fully NFREAs: (1) Lock the planar conformation of the molecular *via* introducing multiple noncovalent interactions (*e.g.*, F···H, S···N, S···O) or utilizing large steric hindrance groups to promote the π-electron delocalization and intramolecular charge transfer; (2) Introduce the bulky side chain, in particular two-dimension structure, to ensure solubility, inhibit excess aggregation and reduce conformation transition; (3) Form a 3D interpenetrating network stacking structure with all IC terminals packing accurately with each other by adjusting the molecular coplanarity or using multiple electron-deficient units, and then facilitating efficient exciton dissociation and charge transport. (4) Expand the absorption region *via* applying both the steric hindrance effect and noncovalent interaction contained. In addition, the successful case of efficient FREAs could be applied in fully NFREAs to tune the absorption spectra, such as constructing asymmetric skeleton, introducing electron-deficient unit in the molecular core, extending conjugation length in the terminal IC groups, *etc.* (5) Reduce the energy loss by increasing the planarity or the effective conjugated length of molecular backbone, and shrinking the energy level offset between donor and acceptor, and applying ternary strategy. The synergetic effect of these strategies could be expected to further optimization of device performance of fully NFREAs. Besides, increasing the steric hindrance effect of the terminal side chain and constructing the planar skeleton are also both effective in improving device stability. Finally, the ideal efficiency-stability-cost balance and the commercialization of OSCs can be expected.

Declaration of competing interest

The authors declare that they have no known competing financial interests or personal relationships that could have appeared to influence the work reported in this paper.

Acknowledgments

The authors gratefully acknowledge the financial support from National Natural Science Foundation of China (NSFC, Nos. 51973169 and 52003209), the Open Project Program of Wuhan National Laboratory for Optoelectronics (No. 2020WNLOKF015), and the Science Foundation of Wuhan Institute of Technology (Nos. K202023 and K202025).

References

[1] R. Søndergaard, M. Hösel, D. Angmo, T.T. Larsen-Olsen, F.C. Krebs, Mater. Today 15 (2012) 36–49.
[2] Y. Li, Acc. Chem. Res. 45 (2012) 723–733.
[3] X. Wan, C. Li, M. Zhang, Y. Chen, Chem. Soc. Rev. 49 (2020) 2828.
[4] M. Riede, D. Spoltore, K. Leo, Adv. Energy Mater. 11 (2021) 2002653.
[5] G. Wang, M. Adil, J. Zhang, Z. Wei, Adv. Mater. 31 (2019) 1805089.
[6] P. Cheng, G. Li, X. Zhan, Y. Yang, Nat. Photon. 12 (2018) 131–142.
[7] J. Hou, O. Inganäs, R.H. Friend, F. Gao, Nat. Mater. 17 (2018) 119–128.
[8] C. Yan, S. Barlow, Z. Wang, et al., Nat. Rev. Mater. 3 (2018) 18003.
[9] Z. Liu, X. Zhang, P. Li, X. Gao, Sol. Energy 174 (2018) 171–188.
[10] J. Wang, X. Zhan, Chin. J. Chem. 40 (2022) 1592–1607.
[11] H. Huang, Q. Guo, S. Feng, et al., Nat. Commun. 10 (2019) 3038.
[12] Y. Cui, H. Yao, J. Zhang, et al., Adv. Mater. 32 (2020) 1908205.
[13] C. Li, J. Zhou, J. Song, et al., Nat. Energy 6 (2021) 605–613.
[14] Q. Liu, Y. Jiang, K. Jin, et al., Sci. Bull. 65 (2020) 272–275.
[15] Z. Luo, R. Ma, J. Yu, et al., Natl. Sci. Rev. 9 (2022) nwac076.
[16] Y. Lin, J. Wang, Z.G. Zhang, et al., Adv. Mater. 27 (2015) 1170–1174.
[17] B. Guo, W. Li, X. Guo, et al., Adv. Mater. 29 (2017) 1702291.
[18] H. Yao, Y. Cui, R. Yu, et al., Angew. Chem. Int. Ed. Engl. 129 (2017) 3091–3095.
[19] Z. Xiao, X. Jia, L. Ding, Sci. Bull. 62 (2017) 1562–1564.
[20] L. Yang, M. Li, J. Song, et al., Adv. Funct. Mater. 28 (2018) 1705927.
[21] Y. Li, L. Zhong, B. Gautam, et al., Energy Environ. Sci. 10 (2017) 1610–1620.
[22] J. Yuan, Y. Zhang, L. Zhou, et al., Joule 3 (2019) 1140–1151.
[23] K. Jiang, Q. Wei, J.Y.L. Lai, et al., Joule 3 (2019) 3020–3033.
[24] Y. Zhang, Y. Ji, Y. Zhang, et al., Adv. Funct. Mater. 32 (2022) 2205115.
[25] M. Zhang, L. Zhu, G. Zhou, et al., Nat. Commun. 12 (2021) 309.
[26] L. Zhan, S. Li, X. Xia, et al., Adv. Mater. 33 (2021) 2007231.
[27] Y. Cui, Y. Xu, H. Yao, et al., Adv. Mater. 33 (2021) 2102420.
[28] L. Zhu, M. Zhang, J. Xu, et al., Nat. Mater. 21 (2022) 656–663.
[29] W. Gao, F. Qi, Z. Peng, et al., Adv. Mater. 34 (2022) 2202089.
[30] R. Sun, Y. Wu, X. Yang, et al., Adv. Mater. 34 (2022) 2110147.
[31] K. Chong, X. Xu, H. Meng, et al., Adv. Mater. 34 (2022) 2109516.
[32] H. Huang, L. Yang, A. Facchetti, T.J. Marks, Chem. Rev. 117 (2017) 10291–10318.
[33] N.E. Jackson, B.M. Savoie, K.L. Kohlstedt, et al., J. Am. Chem. Soc. 135 (2013) 10475–10483.
[34] Y. Liu, Z. Zhang, S. Feng, et al., J. Am. Chem. Soc. 139 (2017) 3356–3359.
[35] X. Wang, H. Lu, Y. Liu, et al., Adv. Energy Mater. 11 (2021) 2102591.
[36] D. Luo, X. Lai, N. Zheng, et al., Chem. Eng. J. 420 (2021) 129768.
[37] X. Liu, Y. Wei, X. Zhang, et al., Sci. China Chem. 64 (2020) 228–231.
[38] H. Yu, Z. Qi, X. Li, et al., Sol. RRL 4 (2020) 2000421.
[39] Z. Wu, Y. Chen, L. Zhang, et al., J. Mater. Chem. A 9 (2021) 3314–3321.
[40] H. Lu, X. Wang, H. Wang, et al., Sci. China Chem. 65 (2022) 594–601.
[41] L. Ma, S. Zhang, J. Zhu, et al., Nat. Commun. 12 (2021) 5093.
[42] Z.P. Yu, Z.X. Liu, F.X. Chen, et al., Nat. Commun. 10 (2019) 2152.
[43] Z.X. Liu, Z.P. Yu, Z. Shen, et al., Nat. Commun. 12 (2021) 3049.
[44] T.J. Wen, Z.X. Liu, Z. Chen, et al., Angew. Chem. Int. Ed. 60 (2021) 12964–12970.
[45] T.J. Wen, J. Xiang, N. Jain, et al., J. Energy Chem. 70 (2022) 576–582.
[46] C. Li, X. Zhang, N. Yu, et al., Adv. Funct. Mater. 32 (2022) 2108861.
[47] Y. Li, Y. Xu, F. Yang, et al., Chin. Chem. Lett. 30 (2019) 222–224.
[48] Z. Yao, Y. Li, S. Li, et al., ACS Appl. Energy Mater. 4 (2021) 819–827.
[49] J. Zhu, C. Yang, L. Ma, et al., Org. Electron. 105 (2022) 106512.
[50] Y.N. Chen, M. Li, Y. Wang, et al., Angew. Chem. Int. Ed. 59 (2020) 22714–22720.
[51] Y. Zhou, M. Li, H. Lu, et al., Adv. Funct. Mater. 31 (2021) 2101742.
[52] X. Zheng, W. Liu, H. Lu, et al., Chem. Eng. J. 444 (2022) 136472.
[53] J. Li, H. Li, L. Ma, et al., Small Methods 6 (2022) 2200007.
[54] Q. Fan, H. Fu, Q. Wu, et al., Angew. Chem. Int. Ed. 60 (2021) 15935.
[55] Z. Zhang, Y. Li, G. Cai, et al., J. Am. Chem. Soc. 142 (2020) 18741–18745.
[56] Z. Liang, M. Li, X. Zhang, et al., J. Mater. Chem. A 6 (2018) 8059–8067.
[57] H. Yu, Z. Qi, J. Zhang, et al., J. Mater. Chem. A 8 (2020) 23756–23765.
[58] X. Ding, X. Chen, Y. Xu, et al., Chem. Eng. J. 429 (2022) 132298.